LIP-STUDENTS-25-12

Analysis of Solar Energetic Proton Events Observed by BERM during the BepiColombo Cruise

Diogo Carvalho[1,a] and Jaime Antunes[1,b]

[1] *Instituto Superior Técnico, Lisboa, Portugal*

Project supervisor: António Pessanha Gomes

September 30, 2025

Abstract. A catalog of solar energetic proton events detected by the BepiColombo Environment Radiation Monitor (BERM) during the cruise phase from October 2018 to July 2025 is presented. Using a conservative statistical identification pipeline, 56 events were isolated, of which 36 meet stricter flux criteria, providing a robust dataset despite significant observational gaps. The catalog enables systematic characterization of SEP occurrence, peak fluxes, durations, and fluence spectra in the inner heliosphere from BepiColombo's vantage point. Event occurrence rates show a clear correlation with solar cycle activity, while peak fluxes scale linearly with integrated fluence but exhibit no consistent relation with duration. Fluence spectra are generally well described by power-law behavior, though deviations suggest more complex forms in some events. No simple dependence on heliocentric distance or spacecraft velocity is observed, underlining the complexity of particle transport. These results establish BERM as a valuable instrument for SEP science, providing both a benchmark dataset and clear directions for cross-mission comparisons, refined event separation, and improved modeling of acceleration and transport processes.

Keywords: SEPs, Energetic Proton Events, BERM, Solar Cycle Dependence, Proton Fluence Spectra

1 Introduction

1.1 Interplanetary Particle Environment

Solar energetic particles (SEPs) are a primary observational tracer of particle acceleration and transport processes in the heliosphere. Their composition, spectra, and temporal evolution provide direct constraints on the physical conditions in the solar corona and interplanetary space (Reames 2013; Schwadron et al. 2017). SEPs constitute a key component of space weather, with implications for the near-Earth environment and the safety of space operations. Understanding the space environment requires characterizing the main populations of energetic particles, including galactic cosmic rays (GCRs), magnetically trapped particles in planetary radiation belts, and SEPs, the signatures of which are the focus of the present data analysis.

Galactic cosmic rays (GCRs) are high-energy charged particles, predominantly protons and some helium nuclei, also including heavier nuclei up to iron, originating outside the Solar System. Their energies range from approximately 10^6 eV to 10^{21} eV, forming a continuous and nearly isotropic background against which SEP enhancements are recognized in situ (Potgieter 2013).

Magnetically trapped particles, mainly protons and electrons, are confined by planetary magnetic fields, forming radiation belts. These populations are well established in the Van Allen belts at Earth and in the intense radiation environment surrounding Jupiter. Mercury, the destination of the mission considered in this work, possesses a weak quasi-magnetosphere, where particles are poorly confined and often lost before completing a full orbit, making their contribution to the local radiation background negligible under the conditions studied (Baker et al. 2018).

[a] e-mail: diogofrcarvalho167@gmail.com
[b] e-mail: jaime.antunes@tecnico.ulisboa.pt

While GCRs and trapped particles form the background radiation, the characteristics and origins of SEPs are introduced in the next section.

1.2 Solar Activity and Particle Acceleration

Solar activity originates in the interaction of plasma motions and magnetic fields in the Sun's outer layers. Differential rotation and convection generate magnetic structures that emerge through the surface and are carried outward by the solar wind, which stretches them into the Parker spiral and defines the large-scale pathways for charged particles (Aschwanden 2005). Magnetic reconnection in active regions provides the basic mechanism for energy release: on closed field lines it produces solar flares, while on open lines it drives plasma jets, both capable of accelerating particles and giving rise to impulsive SEP events (Reames 2013).

Coronal mass ejections (CMEs) represent a more powerful mechanism, ejecting large amounts of plasma at high speeds. When faster than the ambient wave speed, CMEs drive shocks that accelerate protons, electrons, and heavy ions to MeV–GeV energies, producing gradual SEP events that are longer and more widespread (Webb and Howard 2012). The rate of flares and CMEs follows the 11-year solar cycle, with maximum activity leading to frequent SEP events. At the same time, the enhanced heliospheric magnetic field during solar maximum results in stronger solar modulation of GCRs, reducing the observed GCR flux, explaining the observed anticorrelation between SEPs and GCRs (Potgieter 2013).

The seven-year interval considered in this study includes periods of both high and low solar activity, capturing the full range of solar cycle conditions, as presented in Section 2.1.

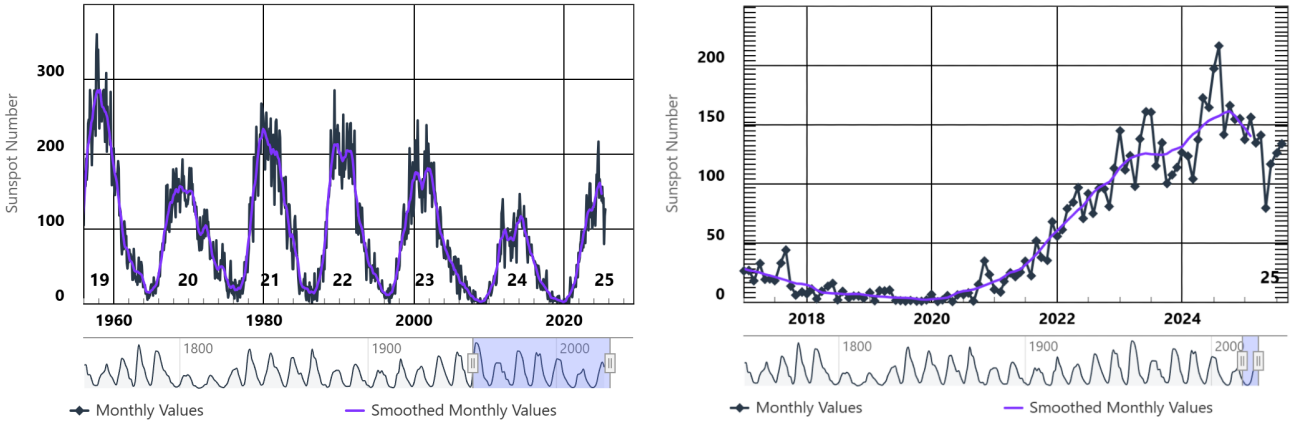

Figure 1: Sunspot number from 1958 to July 2025 (left). Sunspot number over the seven-year period considered in this study, as discussed in Section 2.1 (right). Data from NOAA SWPC (NOAA Space Weather Prediction Center 2025).

1.3 Particle Detection with BERM

The present analysis is based on data collected by the BepiColombo Environment Radiation Monitor (BERM) during the cruise phase of the mission. BERM is a high-energy charged particle detector onboard the Mercury Planetary Orbiter (MPO), part of ESA's BepiColombo mission to Mercury. BepiColombo was launched in 2018 and is scheduled to arrive at Mercury in November 2026, following a cruise phase that includes multiple gravity-assisted flybys of Earth, Venus, and Mercury. The MPO carries a suite of scientific instruments designed to study Mercury's surface, magnetosphere, and radiation environment. BERM is included primarily as a housekeeping instrument to monitor radiation levels, while providing scientific data on energetic particles in interplanetary space during the cruise phase and, subsequently, in the Hermean environment (Pinto et al. 2022).

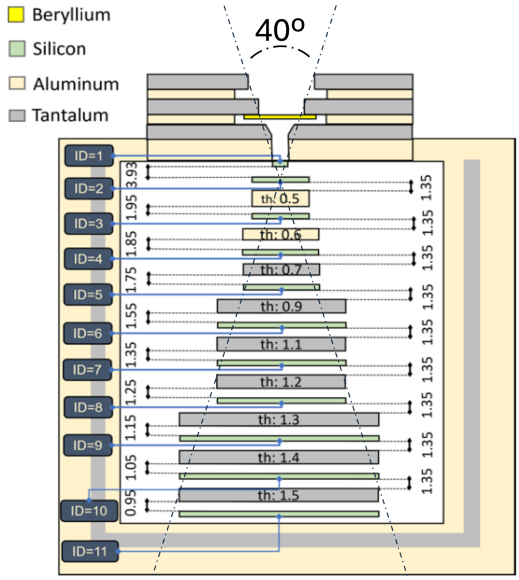

Figure 2: Side view of the BERM detector showing the 11 silicon detectors, tantalum collimator, and shielding. Adapted from Pinto et al. (2022) (Pinto et al. 2022).

BERM is a stack detector composed of 11 silicon layers interleaved with absorbers, with an entrance field of view of 40°. Its beryllium window rejects electrons below 50 keV and protons below 1.35 MeV. Particle identification is organized into five electron channels (0.15–10 MeV), eight proton channels (1.5–100 MeV), and five heavy-ion channels defined by Linear Energy Transfer (LET) from 1 to 50 $MeV^{-1}\,mg^{-1}\,cm^2$, based on the energy deposition pattern across the detector stack. (see Figure 2)

During the cruise phase, BERM operates quasi-continuously, generally pointing antisunward, except when temporarily switched off for operational reasons, which will be specified in the dataset in Section 2.1.

2 Data Analysis

2.1 Dataset

The present study utilizes data from BERM, selected for its continuous coverage of the cruise phase from 2018-10-25 to 2025-07-07, providing a unique record of energetic particle activity in the inner heliosphere prior to Mercury orbital insertion. SEP events are only observed from 2021 onward.

From this year onward, the dataset contains several intervals of instrument inactivity. For interruptions longer than one day, the average gap duration is about 7.4 days, excluding the three longest outages, which are listed separately in Table 1. These extended gaps, each lasting several weeks to months, represent a significant limitation in the temporal coverage of the dataset.

Interval	Start date	End date	Duration (days)
1	2022-01-04	2022-01-24	20.6
2	2024-05-02	2024-08-09	98.9
3	2025-01-16	2025-04-05	79.1

Table 1: Longest BERM inactivity intervals with major impact on SEP statistics from 2021 onwards.

Only proton measurements were considered, while electrons and heavy ions were excluded due to the limited timeframe of the present study. This dataset, even in the absence of multi-spacecraft comparison, allowed the creation of a preliminary catalog of solar energetic proton events and the exploration of statistical relationships between key parameters.

2.2 Event Identification Method

The identification of energetic particle events in the BERM dataset follows a statistical threshold method, where flux measurements in the lowest-energy channel (2.25 MeV, chosen for its higher sensitivity) are compared with quiet-time background levels. Background conditions were estimated from the interval 2024-01-10 to 2024-01-20, selected after inspection of the dataset as representative of stable fluxes with no signatures of SEP activity. From this period, the mean flux and its standard deviation were derived, and the detection threshold was defined as

$$\text{Threshold} = \mu_{\text{background}} + n \times \sigma_{\text{background}} \quad (1)$$

where $\mu_{\text{background}}$ is the mean flux, $\sigma_{\text{background}}$ is the standard deviation, and n is a constant controlling the sensitivity of the identification. An event is recorded when the flux in at least one of the selected energy channels exceeds this threshold. Once triggered, the event remains active until the flux stays below the threshold for more than 10 h, preventing premature termination due to transient fluctuations. Events shorter than 5 h are discarded, as they are typically inconsistent with SEP signatures.

Candidate events are then refined using a local background calculated from a quiet interval preceding each event. The refined catalog is obtained by applying the following criteria: a 3-day background window, $n = 6$, minimum below-threshold duration of 15 hours, and a minimum gap duration of 1 day. From this refined list, a filtered catalog is generated by imposing a single stricter criterion: a minimum peak flux of 45 $\text{cm}^{-2}\,\text{s}^{-1}\,\text{sr}^{-1}\,\text{MeV}^{-1}$.

This procedure results in two complementary event catalogs: the refined list captures all statistically significant events according to the defined thresholds and durations, while the filtered list highlights the subset of the most prominent events based on peak flux. For each event, key parameters, including peak flux, rise and decay times, fluence, and associated uncertainties, were extracted across all energy channels and stored in machine-readable format for subsequent statistical analysis.

2.3 Statistical Analysis

The statistical analysis was performed on both the refined and filtered event datasets. Histograms of maximum fluxes were constructed for each energy channel, while event durations and survival functions were analyzed to characterize the basic statistical properties. Event occurrence rates were aggregated annually and corrected for detector uptime to examine correlations with sunspot numbers and the solar cycle.

Event parameter relationships were also examined to assess how event intensity relates to both the integrated particle fluence and the temporal characteristics of the events.

Cumulative fluence over time was evaluated to quantify the integrated particle exposure, followed by Pareto analysis to assess the contribution of the most intense events to the total fluence. Fluence spectra were fitted with a power-law

$$F(E) = A \times E^{-\gamma} \quad (2)$$

with the spectral index γ extracted for statistical comparison across events.

Finally, event properties were evaluated as a function of spacecraft distance and velocity to evaluate potential effects of particle propagation on the observations.

3 Results

3.1 Identified Events

In the initial identification stage, a total of 565 candidate events were identified. After applying the refinement procedure, this number was reduced to 56, and following the application of the filtering criteria, 36 events remained. The large number of candidates in the first step reflects the sensitivity of the method, which was kept unchanged to maximize the chance of capturing possible events. Most preliminary identifications correspond to background fluctuations. However, by recalculating the background in the interval preceding each event, the refinement step effectively distinguishes genuine SEP signatures from spurious detections, resulting in a more robust dataset. An illustrative example of this refinement process is shown in Figure 3.

The resulting catalog, while providing a consistent set of detected events, is subject to several methodological constraints that must be considered when interpreting the following results. A first limitation concerns the aggregation of multiple solar events into a single detection. When consecutive or overlapping injections of particles arrive at the spacecraft, their flux signatures combine, producing complex profiles with peaks and depressions that do not return to background levels between episodes. In such cases, the identification procedure records a single extended event, rather than resolving the individual contributions from distinct solar eruptions.

A second source of uncertainty lies in the definition of event boundaries. First, the local background selected by the algorithm may be affected by residual fluctuations, leading to a threshold level that does not fully represent quiet conditions. In the initial stage, several hundred candidate events are identified. Although many of these detections are later discarded during refinement, their associated background intervals are still used in the analysis.

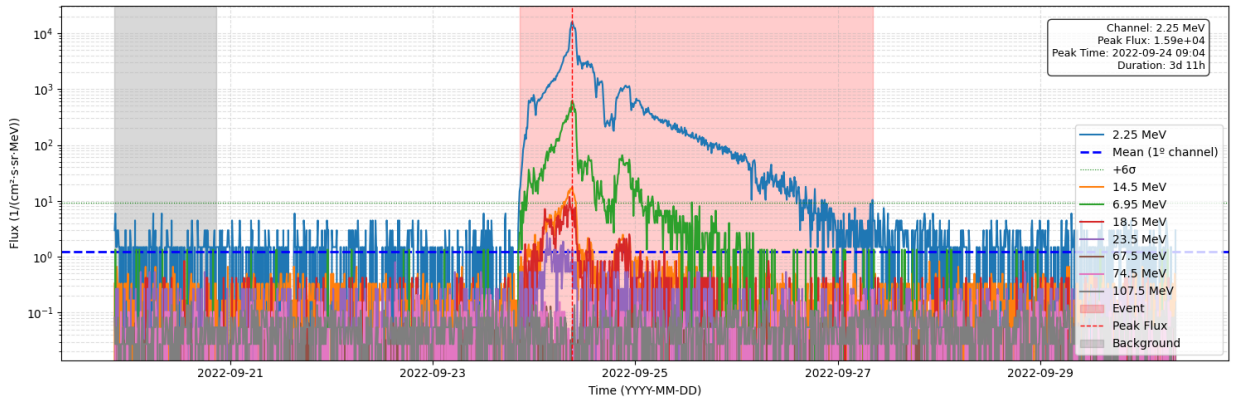

Figure 3: Solar energetic proton event detected by BERM between 2022-09-23 and 2022-09-27, included in both the refined and filtered catalogs described in Section 2.2. The shaded band indicates the background level estimated by the identification method.

This approach ensures that the background estimation is more robust: even if some intervals fall within the tail of a neighboring event, others provide a more reliable representation of quiet conditions. When these detections are subsequently merged, the overlapping backgrounds constrain the boundaries, so that the resulting event typically starts earlier and ends later than any individual candidate, yielding a more conservative definition of the true event.This can shift both onset and termination times. In addition, because the method relies on a statistical tolerance factor, slow decays can drop below the threshold before the particle population has fully returned to baseline, resulting in shortened durations. Together, these effects introduce systematic uncertainties in onset and end times, as well as in derived quantities such as fluence and cumulative exposure.

These limitations reflect the fact that the catalog is not a direct inventory of solar eruptions, but rather a characterization of the SEP signatures as observed from the spacecraft perspective, shaped by the detection method and its statistical parameters.

3.2 Catalogue Characterization

To provide an overview of the event population, the distributions of peak fluxes and event durations were analyzed using the refined catalog. This ensures that the statistics capture all significant detections without imposing additional selection on event intensity.

The histogram of peak fluxes (logarithmic scale) shows that most detections cluster at low intensities, with a clear break around the 70th percentile (3.99×10^2 cm^{-2} s^{-1} sr^{-1} MeV^{-1}), indicating that moderate SEP events dominate while strong events are comparatively rare. (Figure 4)

Event durations are similarly skewed (Figure 4). Most events last less than one week, with the 90th percentile at 6.22 days, while a few outliers extend to approximately two weeks, consistent with aggregated detections as discussed in Section 3.1. The Kaplan–Meier survival curve confirms this pattern, showing a nearly linear decline up to about 6 days, followed by a slow decay with extended plateaus. These observations indicate a SEP population dominated by short-to-moderate events, with long or intense events confined to the upper tails of the distributions.

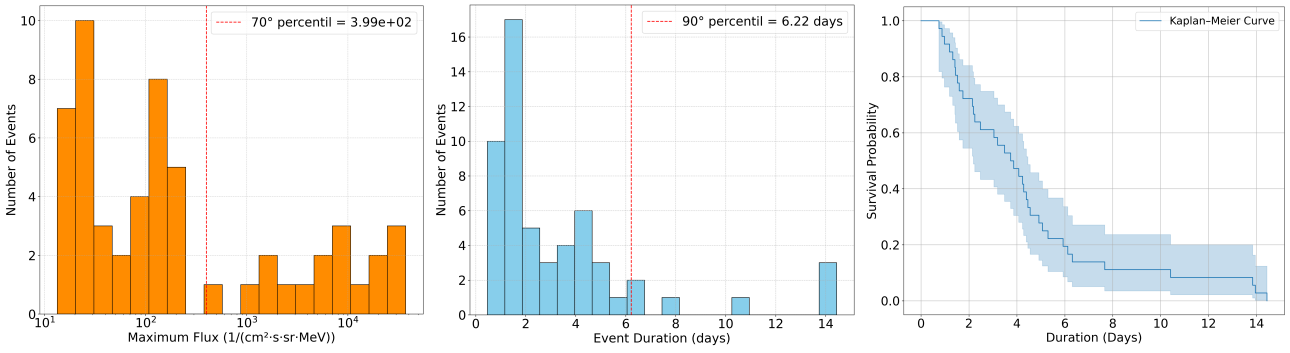

Figure 4: Distribution of peak proton fluxes in the 2.25 MeV channel of BERM for the refined event catalog (left). Distribution of event durations in the refined catalog (center). Kaplan–Meier survival curve of event durations, illustrating the probability of event persistence over time (right).

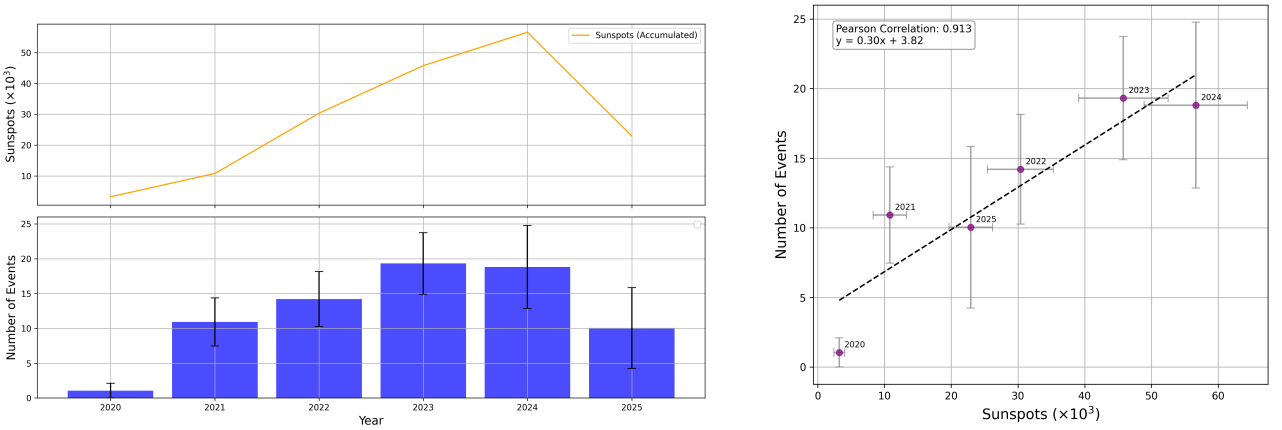

Figure 5: Annual number of SEP events identified from BERM measurements, corrected for instrument operational time, compared with the annual sunspot number (left). Correlation between annual SEP event counts identified from BERM data and annual sunspot numbers (right).

3.3 Solar Activity Correlations

The occurrence of SEP events detected by BERM was analyzed in relation to the solar cycle, represented by the annual sunspot number, using the refined catalog to encompass the full range of event intensities. Event counts were corrected for operational time using

$$n_{corrected} = \frac{365}{\text{active days}} \times n_{events} \tag{3}$$

with the same factor applied to the associated uncertainties.

The annual event counts generally follow the trend of sunspot numbers, as shown in the left panel of Figure 5. In 2024, however, no clear increase relative to 2023 is observed due to a prolonged BERM inactivity (Table 1), which limited the detection of events despite the applied correction. This effect is reflected in the enlarged error bars and in the position of 2024 below the regression line in the right panel of Figure 5. A similar discrepancy occurs in 2025, reflecting incomplete coverage up to July and further operational gaps. Despite these limitations, the correlation remains statistically strong, with a Pearson coefficient of 0.792.

The relationship between mean peak flux and solar activity, illustrated in Figure 6, shows a general tendency for higher fluxes at solar maximum. However, the distribution includes an outlier in 2023, where unusually low average fluxes were recorded, deviating from the expected trend. The physical origin of this discrepancy is unclear. It may reflect heliospheric variability, detection limitations, or statistical fluctuation. Future analyses, including cross-mission comparisons, will be needed to clarify this.

In Figure 7, the corrected fluence, defined as the event-integrated flux minus the preceding background, was compared with sunspot numbers. The Pearson correlation is 0.673, primarily influenced by the 2023 outlier mentioned above, whereas the remaining points generally follow a linear trend.

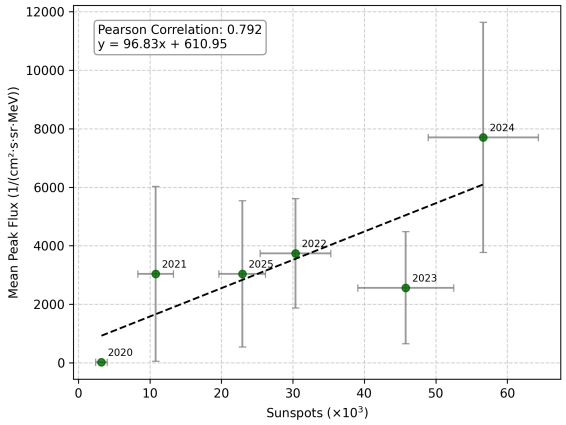

Figure 6: Mean peak proton flux of identified SEP events as a function of annual sunspot numbers.

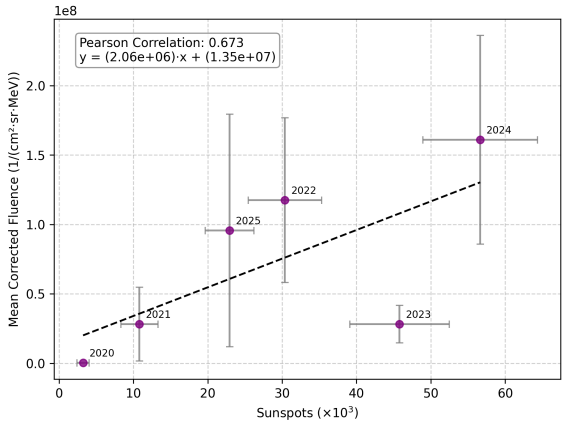

Figure 7: Mean corrected fluence of identified SEP events compared with annual sunspot numbers.

A clearer trend emerges for mean event duration, shown in Figure 8. Here, the correlation with sunspot numbers is particularly strong (Pearson coefficient 0.988), suggesting that higher solar activity is associated with longer events. However, part of this trend may result from the aggregation of overlapping events during periods of intense solar activity, as discussed in Section 3.1.

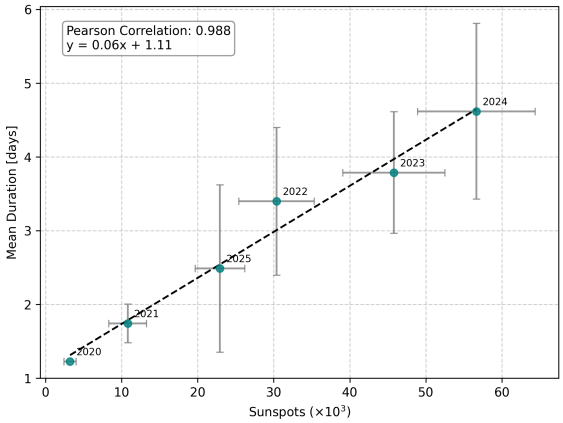

Figure 8: Mean duration of identified SEP events as a function of annual sunspot numbers.

3.4 Event Parameter Correlations

The relationships between key event parameters were investigated to assess how event intensity relates to both integrated particle fluence and event duration.

A pronounced linear relationship is observed between peak flux and integrated fluence (Pearson correlation 0.956) in Figure 9, indicating that more intense events generally contribute proportionally more to the total particle exposure. Although the dataset is more densely populated at lower flux and fluence values, a sufficient number of high-energy events are present to support the validity of this relationship across the full energy range.

By contrast, peak flux shows no systematic relationship with event duration (Pearson correlation 0.625), as illustrated in Figure 10. This analysis aimed to explore whether the peak magnitude could provide predictive information on the temporal extent of an event, given that rise phases are typically faster than decay phases. The lack of correlation arises in part because many events reach their peak late due to the aggregation of overlapping events, as previously discussed. Apart from the absence of very short events with high peak flux, the data exhibit substantial scatter, indicating that peak intensity alone is not a reliable predictor of event duration.

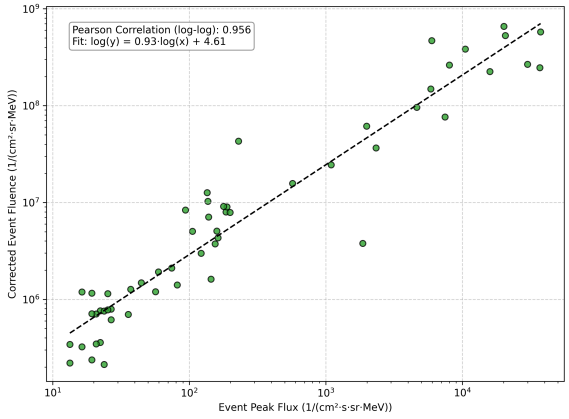

Figure 9: Fluence as a function of Peak proton flux for identified SEP events.

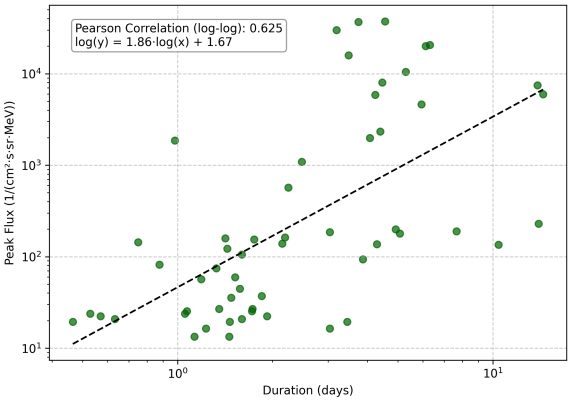

Figure 10: Peak proton flux as a function of event duration for identified SEP events.

3.5 Spectral and Fluence Analysis

The contribution of individual SEP events to the total particle fluence was analyzed to characterize both the temporal evolution of fluence and the relative impact of high-intensity events.

The cumulative fluence (left panel of Figure 11) shows a non-uniform increase over the observation period. In 2023, fluence accumulation is limited despite continuous BERM operation, while 2024 exhibits two distinct sharp rises, consistent with enhanced solar activity. The following horizontal segments in the curve correspond to periods of instrument inactivity, particularly during high-activity phases, which may have led to underestimation of the total fluence during these intervals.

The Pareto analysis (right panel of Figure 11) further illustrates the distribution of fluence among events. Approximately 20% of events contribute nearly 80% of the total accumulated fluence, highlighting the dominance of a small number of high-intensity events. Operational gaps occurring during periods of elevated solar activity reduce the representation of the most energetic events in the dataset, potentially affecting the cumulative contribution of these events to the overall fluence distribution.

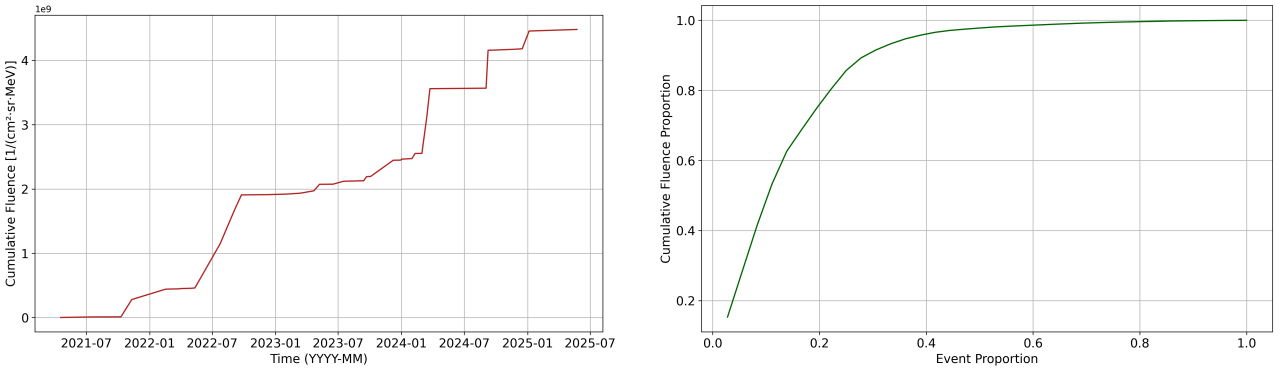

Figure 11: Accumulated proton fluence over the observation period, showing the temporal contribution of individual SEP events (left). Pareto analysis of SEP events, showing that approximately 20% of events contribute 80% of the total fluence (right).

To investigate the energy dependence of SEP events, fluence spectra were fitted with power-law models. This analysis was restricted to the filtered dataset, since only events with sufficiently high peak fluxes provide well-resolved, low-noise spectra. Fluence values were corrected for each of the five BERM proton channels, as described earlier, and a set of quality criteria was imposed to ensure statistical robustness. Only data points with positive fluence and with relative uncertainties not exceeding 50% of the fluence value were retained. Monotonic decrease of fluence with increasing energy was enforced, and points statistically indistinguishable from their predecessors were discarded. A minimum of three valid channels was required to allow a reliable single power-law fit.

Out of the 36 candidate events, 32 satisfied these requirements. Events were excluded primarily due to inconsistencies between adjacent intermediate-energy channels or insufficient data points after filtering. For the selected events, the majority of spectra were well described by power-law behavior across the available energy range. An illustrative case is shown in Figure 12.

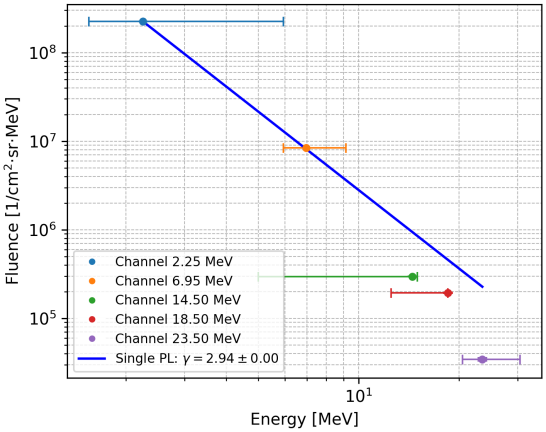

Figure 12: Fluence spectrum of the SEP event detected by BERM between 2022-09-23 and 2022-09-27, corresponding to the event shown in Figure 3. The solid line indicates the best-fit single power-law model applied to the corrected fluence values across the five proton channels.

In several other cases, however, the high-energy channels lay systematically below the extrapolation of the best-fit curve, suggesting that a broken power-law may better represent certain events, reflecting the complex physical processes shaping particle propagation and acceleration.

The distribution of derived spectral indices is summarized in the Figure 13 . Most events cluster between −3.0 and −2.5, with a pronounced peak in this range. Less frequent occurrences extend toward steeper spectra, down to about −5.5, while a small number of events exhibit harder spectra up to −1.5. This distribution shows that the majority of SEP events detected by BERM are characterized by moderately steep fluence spectra. The presence of both softer and harder tails reflects event-to-event variability, possibly linked to differences in acceleration efficiency, shock strength, or interplanetary transport conditions.

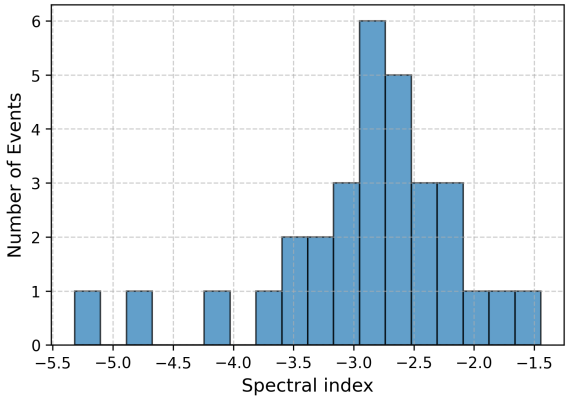

Figure 13: Histogram of power-law spectral indices derived from the corrected fluence spectra of the filtered events.

3.6 Orbital Dependence of Event Properties

The relationship between event intensity and spacecraft heliocentric distance was first examined through peak flux analysis. Although a decrease in intensity with increasing distance from the Sun might be expected, the data revealed only a broad scatter without a clear dependence. This reflects the intrinsic diversity of SEP events, whose intensities are shaped by both source conditions and interplanetary transport effects. From a single-spacecraft perspective, such variability masks any systematic radial trend.

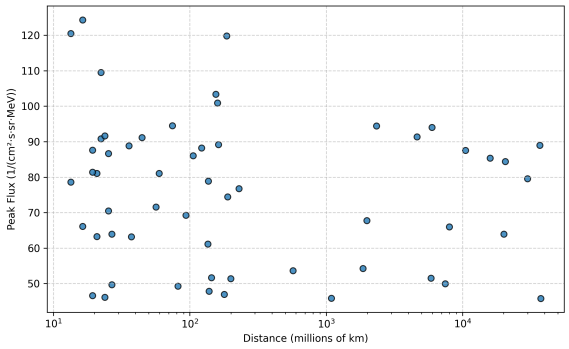

Figure 14: Peak flux of events as a function of spacecraft heliocentric distance.

The potential influence of spacecraft speed on the apparent duration of events was also assessed. The hypothesis was that faster orbital motion could yield shorter observed durations, as the spacecraft would traverse particle-filled flux tubes more rapidly. No consistent relation was found, with the results instead showing strong dispersion. This outcome arises from the complex interaction between spacecraft motion and the structure of particle populations, where wide regions can lead to long durations regardless of orbital speed, while narrower ones may appear brief even at lower velocities.

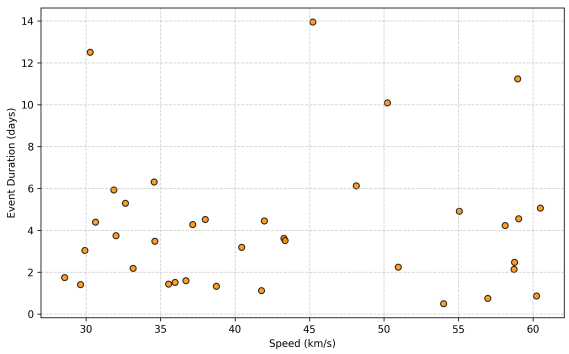

Figure 15: Duration of events as a function of spacecraft velocity

4 Conclusions and Future Work

This study establishes a preliminary catalog of solar energetic proton events detected by BERM during the Bepi-Colombo cruise phase, offering a coherent basis for analyzing event occurrence, intensities, durations and spectra in the inner heliosphere.

The detection pipeline used here is transparent and conservative. To improve the separation of aggregated injections, complementary approaches such as gradient-based detection should be applied in follow-up work in order to obtain more reliable solar-referenced onsets and ends.

Observed correlations with solar activity are informative but affected by uneven coverage and a few anomalous years. Future corrections should combine per-day detection rates with a formal treatment of statistical uncertainties, making use of models that account for variability in event counts and propagating errors through Monte Carlo methods. Comparing the catalog with contemporaneous proton measurements from other missions will help determine whether apparent outliers are instrumental or heliospheric.

Relations among event parameters show clear signals and clear limitations. Peak flux correlates strongly with integrated fluence and remains a useful exposure proxy. The connection between peak flux and duration is less certain. Building a subset of events with accurately constrained solar onsets and ends, guided by other solar observations, will reduce bias from aggregated profiles and enable clearer tests of temporal physics.

Integrated fluence spectra capture average behavior, but spectra evaluated near event peak will be less affected by uncertain tails. Formal comparison of single power laws and broken power laws with model selection criteria will clarify when spectral breaks are statistically justified and when they carry physical meaning about acceleration or transport.

The absence of simple radial or velocity trends in this single-spacecraft record highlights the limits of lone measurements for separating source, transport and geometry effects. Coordinated observations at different heliocentric positions and targeted transport modeling are needed to move from statistical description to a clearer understanding of the underlying processes.

Expanding the analysis to include electron and heavy ion channels with careful calibration and contamination assessment will widen compositional and timing diagnostics and increase the catalog's scientific reach. Taken together with improved event separation, formal treatments of statistical uncertainties, peak-centered spectral analysis, and coordinated comparisons across missions, these steps define a clear path toward a deeper understanding of the processes that govern solar energetic particle acceleration, transport and variability.

Acknowledgements

The authors acknowledge LIP for providing the opportunity to undertake this internship, which offered valuable exposure to the research environment and methodologies in experimental physics. The support of the SpaceRad group is also acknowledged for their guidance and for introducing us to the field of astrophysical particle studies. Particular thanks are due to our supervisor, António Gomes, for his continuous mentorship, constructive feedback, and guidance throughout the project, which greatly contributed to the development of our research skills. This work was supported by the project "Advanced Methods for Solar Energetic Particle Events Characterization in the Inner Solar System" (UI/BD/154742/2023), and by the European Space Agency under contract No. 4000137865/22/ES/JD — Expert Support to BERM & RADEM units.

References

Aschwanden, Markus (2005). *Physics of the Solar Corona*. Berlin: Springer. ISBN: 3-540-30765-6.

Baker, D. N. et al. (2018). "Space Weather Effects in the Earth's Radiation Belts". In: *Space Science Reviews* 214, p. 17. DOI: 10.1007/s11214-017-0452-7.

NOAA Space Weather Prediction Center (2025). *Solar Cycle Progression*. Accessed July 2025. URL: https://www.swpc.noaa.gov/products/solar-cycle-progression.

Pinto, M. et al. (2022). "The BepiColombo Environment Radiation Monitor, BERM". In: *Space Science Reviews* 218. DOI: 10.1007/s11214-022-00922-2.

Potgieter, M. S. (2013). "Solar Modulation of Cosmic Rays". In: *Living Reviews in Solar Physics* 10.3. DOI: 10.12942/lrsp-2013-3.

Reames, D. V. (2013). "The two sources of solar energetic particles". In: *Space Science Reviews* 175, pp. 53–92. DOI: 10.1007/s11214-013-9958-9.

Schwadron, N. A. et al. (2017). "Particle Radiation Sources, Propagation and Interactions in Deep Space, at Earth, the Moon, Mars, and Beyond". In: *Space Science Reviews* 212, pp. 1069–1106. DOI: 10.1007/s11214-017-0381-5.

Webb, D. F. and T. A. Howard (2012). "Coronal mass ejections: observations". In: *Living Reviews in Solar Physics* 9.3. DOI: 10.12942/lrsp-2012-3.